

Interactions and dynamics of one-dimensional droplets, bubbles and kinks

G. C. Katsimiga,¹ S. I. Mistakidis,^{2,3} B. A. Malomed,^{4,5}
D. J. Frantzeskakis,⁶ R. Carretero-González,⁷ and P. G. Kevrekidis¹

¹*Department of Mathematics and Statistics, University of Massachusetts, Amherst, MA 01003-4515, USA*

²*ITAMP, Center for Astrophysics | Harvard & Smithsonian, Cambridge, MA 02138 USA*

³*Department of Physics, Harvard University, Cambridge, Massachusetts 02138, USA*

⁴*Department of Physical Electronics, School of Electrical Engineering,*

Faculty of Engineering, Tel Aviv University, Tel Aviv 69978, Israel

⁵*Instituto de Alta Investigación, Universidad de Tarapacá, Casilla 7D, Arica 1000000, Chile*

⁶*Department of Physics, National and Kapodistrian University of Athens,*

Panepistimiopolis, Zografos, Athens 15784, Greece

⁷*Nonlinear Dynamical Systems Group, Computational Sciences Research Center,*

and Department of Mathematics and Statistics, San Diego State University, San Diego, California 92182-7720, USA

We explore the dynamics and interactions of multiple bright droplets and bubbles, as well as the interactions of kinks with droplets and with antikinks, in the extended one-dimensional Gross-Pitaevskii model including the Lee-Huang-Yang correction. Existence regions are identified for the one-dimensional droplets and bubbles in terms of their chemical potential, verifying the stability of the droplets and exposing the instability of the bubbles. The limiting case of the droplet family is a stable kink. The interactions between droplets demonstrate in-phase (out-of-phase) attraction (repulsion), with the so-called Manton’s method explicating the observed dynamical response, and mixed behavior for intermediate values of the phase shift. Droplets bearing different chemical potentials experience mass-exchange phenomena. Individual bubbles exhibit core expansion and mutual attraction prior to their destabilization. Droplets interacting with kinks are absorbed by them, a process accompanied by the emission of dispersive shock waves and gray solitons. Kink-antikink interactions are repulsive, generating counter-propagating shock waves. Our findings reveal dynamical features of droplets and kinks that can be detected in current experiments.

I. INTRODUCTION

Quantum droplets are self-bound many-body states emanating from the competition between mean-field and quantum-fluctuation energy contributions [1], which crucially depend on the system’s dimensionality [2]. Droplets have been first observed in dipolar atomic condensates [3, 4] and then in bosonic mixtures with contact interactions, under the action of external confinement [5–7] and in free space [8]. Quantum fluctuations are commonly modeled by the Lee-Huang-Yang (LHY) term [9] added to the mean-field Gross-Pitaevskii equations (GPEs) [1, 10]. The accordingly amended GPEs have been successfully applied for the description of droplet structures and dynamics [11–13], including their collective response [14–17], thermal [18, 19] and modulational [20–22] instabilities, as well as the capability to maintain robust self-trapping in the soliton [23–25] and vortex [26, 27] states. Droplets are filled by an extremely dilute quantum fluid. Because the density is limited by a maximum value admitted by the competition between the mean-field attraction and LHY repulsion, the increase of the number of atoms bound in the droplets leads to the formation of their flat-top shapes [1]. This is in sharp contrast to other quantum self-bound states, such as liquid-Helium drops [28, 29] which feature densities at least six orders of magnitude higher than quantum droplets.

More recently, it was found that, besides the droplets, similar states exist at relatively low chemical poten-

tials. While their density profiles resemble dark solitons, they typically feature a substantially larger width and no phase jump. Those states are dubbed bubbles [23] hereafter in the present work. These structures are represented by homoclinic solutions attached to potential maxima in the corresponding phase space, as is shown in the discussion below. In contrast to self-confined (“bright”) droplets, the excitation spectra and dynamical response of bubbles are largely unexplored, which is one of the foci of the present work. Notice that exploring the excitation spectrum for the bright droplets [14] reveals that, under specific conditions, upon tuning the interactions the droplets tend to “cool down”, i.e., it is not energetically favorable for the droplet to be in an excited state.

An important open question concerns the interaction among droplets and that between bubbles, as well as the fate of droplets colliding with other structures, such as kinks [26]. An interesting prospect here is to develop an effective particle-like dynamical picture, similar to how it was done previously for solitary waves [30–33], aiming to capture quantitative aspects of interactions between the droplets. Collisions of 3D droplets in ³⁹K [34] have been experimentally monitored. It was demonstrated that two slowly colliding droplets merge into a single one, while fast collisions are quasi-elastic. A theoretical analysis argued that these outcomes may be attributed to effective range interactions and selective three-body recombination processes in the condensate [35]. The same categorization of collisions has also been demonstrated

theoretically in 2D [36], although the latter can feature more than two droplets as a dynamical outcome. The work of Ref. [37] argued that tuning the relative velocity, phase shift, and atom number allows the colliding droplets to merge or even fragment. Similar effects, i.e., elastic or inelastic collisions, take place in the presence of spin-orbit coupling [38]. The scattering of effectively 1D bright droplets on a potential barrier or well leads to splitting into transmitted, reflected, and trapped fractions, depending on the initial velocity and atom number of the droplet [39]. It is also of particular importance to understand if, similarly to what is well known for usual 1D solitons, interacting droplets attract or repel each other, depending on their relative phase difference.

In the present work, we start by revisiting the stability properties of one-dimensional droplets [14]. Here, we benchmark the droplet stability throughout their interval of existence in terms of the chemical potential. By analyzing the relevant dynamical system, well-defined boundaries between the existence of droplets and bubbles are identified, varying the chemical potential. The linear spectrum of small perturbations is computed for bubbles, demonstrating their instability, which dynamically manifests itself via expansion of their core.

Turning to interactions between droplets, we conclude that they are pairwise-attractive (repulsive) when the droplets are in-phase (out-of-phase). For well-separated in- and out-of-phase droplets we develop the so-called Manton’s method [31] that quantifies their interaction force. Very good agreement of this particle-like picture with the amended GPE predictions is showcased. One can observe accordingly an initial attraction for the case of phase differences between 0 and $\pi/2$, while, on the other hand, repulsion is prevalent for relative phases between $\pi/2$ and π . Moreover, the interactions appear to be more complex and mass exchange between interacting droplets with different chemical potentials occurs. Interactions between bubbles are sensitive to their relative distance. They can either lead to a merger, i.e., a heavier bubble, while emitting counter-propagating shock waves, or to individual core expansion of each bubble, creating a bright droplet in-between. On the other hand, droplets are attracted to and subsequently “absorbed” by kinks, a process followed by the nucleation of dispersive shock waves and the downstream emission of gray solitons. Kink-antikink interactions are found to be repulsive. This interaction is accompanied by the spontaneous emission of counter-propagating shock waves. The above constitute the prototypical interaction features identified in the present manuscript.

This work is organized as follows. Section II introduces the theoretical framework in terms of the LHY-amended GPEs, the linearized (Bogoliubov-de Gennes) equations for small perturbations, and the effective interaction potential for droplets and bubbles. We elaborate on the stability of bright droplets and bubbles in Secs. III and IV, respectively. The droplet-droplet, bubble-bubble, and droplet-kink interactions and their dependence on the

relative distance, phase shift, and chemical potential of the interacting modes are addressed in Sec. V. We provide a summary and discuss future research directions in Sec. VI.

II. DROPLET AND BUBBLE SETTINGS

A. The extended Gross-Pitaevskii equation

In what follows, we assume a homonuclear mass-balanced ($m_1 = m_2 \equiv m$) mixture of bosonic atoms in two different hyperfine states, experiencing equal intra-component repulsion ($g_{11} = g_{22} \equiv g$) and intercomponent attraction, $g_{12} < 0$. As argued in Refs. [23, 40], this setting naturally supports self-confined (“bright”) droplet and bubble modes at different values of the chemical potential. Experimentally, such a mixture can be realized in free space by employing, in particular, the hyperfine states, $|F, m_F\rangle = |1, -1\rangle$ and $|F, m_F\rangle = |1, 0\rangle$ of ^{39}K as demonstrated in Ref. [8] for the respective 3D setting. Under the above-described symmetry arguments, the two-component system coalesces into a single GPE [1, 10] supplemented by the LHY term, reduced to the 1D quadratic form. The latter term represents the attractive interaction in this limit [13] and the respective 1D amended GPE is given by

$$i\hbar\psi'_{t'} = -\frac{\hbar^2}{2m}\psi'_{x'x'} + \delta g|\psi'|^2\psi' - \frac{\sqrt{2m}}{\pi\hbar}g^{3/2}|\psi'|\psi'. \quad (1)$$

Here, $\psi'(x', t') \equiv \psi'_1 = \psi'_2$ represents the wave function of both components whereas $\delta g = g_{12} + g$ describes the balance of mean-field intracomponent repulsion and intercomponent attraction [1, 13]. The effective interaction strengths are experimentally tunable by dint of the Fano-Feshbach [41] or confinement-induced resonances [42], see also Ref. [8] for the magnetic-field dependence of the scattering lengths in ^{39}K . The energy of the system is measured in units of $\hbar^2/(m\xi^2)$, where $\xi = \pi\hbar^2\sqrt{|\delta g|}/(mg\sqrt{2g})$ is the healing length. Rescaling time, length, and wave function as $t' = \hbar/(m\xi^2)$, $x' = \xi x$ and $\psi' = (2\sqrt{g})^{3/2}\psi/(\pi\xi(2|\delta g|)^{3/4})$, respectively, Eq. (1) can be cast in the dimensionless form

$$i\psi_t = -\frac{1}{2}\psi_{xx} + |\psi|^2\psi - |\psi|\psi. \quad (2)$$

In the following, we focus on the stability and interactions of both droplets and bubbles. It is the balance between the residual mean-field repulsion, LHY attraction and the kinetic energy which allows the self-trapping of stable droplets in free space, see also Ref. [14]. While our findings, as reported below, persist in the presence of a weak external trap, here we restrict the discussion to the most fundamental setting that does not include an external potential. Typical evolution times of $t \sim 10^3$ in the scaled units, that we consider here, translate, in a typical experimental setup [43], with the perpendicular trap $\omega_{\perp} = 2\pi \times 250$ Hz, into 600 ms in physical units.

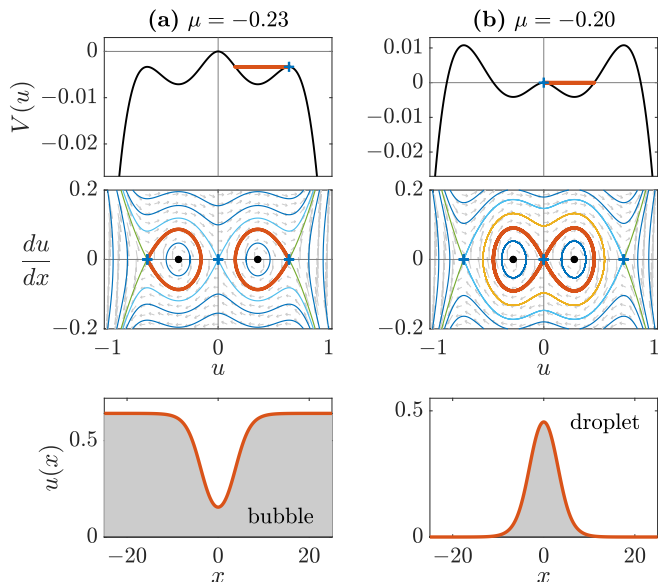


FIG. 1. Self-localized nonlinear structures (see thick red curves) supported by the LHY correction. Typical (a) bubble and (b) droplet solutions (bottom panels) corresponding to two types of homoclinic connections (middle panels) stemming from the Newtonian effective potential reduction (top panels). The bubble refers to a homoclinic connection anchored at the non-zero u_+ constant background while the droplet represents a homoclinic connection of the zero ($u_* = 0$) background.

B. The effective-potential picture and existence regions of droplets and bubbles

When seeking for stationary-state solutions of Eq. (2), the usual ansatz $\psi(x, t) = e^{-i\mu t}u(x)$ is employed, leading to the second-order ordinary differential equation (ODE) —or 2D (Hamiltonian) dynamical system—

$$\frac{d^2u}{dx^2} = 2|u|^2u - 2|u|u - 2\mu u, \quad (3)$$

where x plays the role of the evolution variable [23]. Without loss of generality for our 1D problem, we may assume that the stationary solutions are real, reducing Eq. (3) to the Newtonian equation of motion for a unit-mass particle with coordinate u experiencing the effective potential

$$V(u) = \mu u^2 + \frac{2}{3}u^2|u| - \frac{1}{2}u^4. \quad (4)$$

Characteristic profiles of $V(u)$ are shown in Fig. 1 for two chemical potentials. The fixed points of this potential correspond to

$$u_* = 0 \quad \text{and} \quad u_{\pm} = \frac{1 \pm \sqrt{1 + 4\mu}}{2}. \quad (5)$$

The homogeneous state associated with u_- is modulationally unstable [20], therefore we do not consider it

here. On the other hand, both u_* and the homogeneous state u_+ are modulationally stable, with the latter arising at $\mu = -1/4$ through a saddle-center bifurcation (together with u_-), as seen in Eq. (5). Then, the shape of the effective potential $V(u)$ defined by Eq. (4) determines the nature of the solitonic states that can exist in this setting. Specifically, local maxima of $V(u)$ located at $\pm u_+$ and u_* have equal heights at $\mu = -2/9$.

Turning to the case of $-1/4 < \mu < -2/9$, when the maximum of $V(u)$ at $u = u_*$ is higher than that at $u = \pm u_+$ [top panel of Fig. 1(a)], Eq. (3) produces a bubble (or its negative) homoclinic [i.e., tending asymptotically to the same steady state from the Greek “κλίνω” (to tend) and “ὁμοιο” (same)] to u_+ , see red curves in the middle and bottom panels of Fig. 1(a). For chemical potentials in the interval $-2/9 < \mu < 0$, where the maxima at $\pm u_+$ are higher than the one at u_* [top panel in Fig. 1(b)], there exists a bright droplet [in addition to a heteroclinic dark-soliton state that has been examined elsewhere [40]; heteroclinic stems from “κλίνω” and “ἕτερο” (different), i.e., tending asymptotically to different steady states], see red curves in the middle and bottom panels in Fig. 1(b). For $\mu = 0$, the homogeneous states u_- and u_* collide through a subcritical pitchfork bifurcation [23] and, finally, at $\mu > 0$ the equilibrium point at $u_* = 0$ becomes a local minimum of the potential. In the latter case, the situation is similar to that known for the cubic nonlinear Schrödinger (NLS) equation and it is not considered further herein. As elaborated below, the states of interest, namely bubbles and “bright” droplets exist, respectively, for $-1/4 < \mu < -2/9$ and $-2/9 < \mu < 0$. These chemical potential intervals will be our main focus, in addition to the separatrix value of $\mu = -2/9$ where kinks and antikinks exist.

C. The Bogoliubov-de Gennes linearized equations

To address the stability of droplets and bubbles, Eq. (2) is linearized for small perturbations (f, g) around the respective stationary solution $u_0(x)$. This is done via the ansatz:

$$\psi(x, t) = u_0(x) + \epsilon [f(x, t) + ig(x, t)],$$

yielding the following Bogoliubov-de Gennes (BdG) equations

$$\frac{\partial f}{\partial t} = L_1 g \equiv \left[-\frac{1}{2} \frac{\partial^2}{\partial x^2} - F(u_0^2) \right] g, \quad (6a)$$

$$\frac{\partial g}{\partial t} = -L_2 f \equiv \left[\frac{1}{2} \frac{\partial^2}{\partial x^2} + F(u_0^2) + 2u_0^2 F'(u_0^2) \right] f, \quad (6b)$$

where $F(y) = -y + \sqrt{y}$. L_1 and L_2 are the self-adjoint linearization operators with domain $D(L_1) = D(L_2) = H^2(\mathbb{R})$ while the adopted notation was previously introduced, e.g., in Refs. [44, 45]. Using a separation of variables of the eigenfunctions $(f, g)^T$ (where T denotes

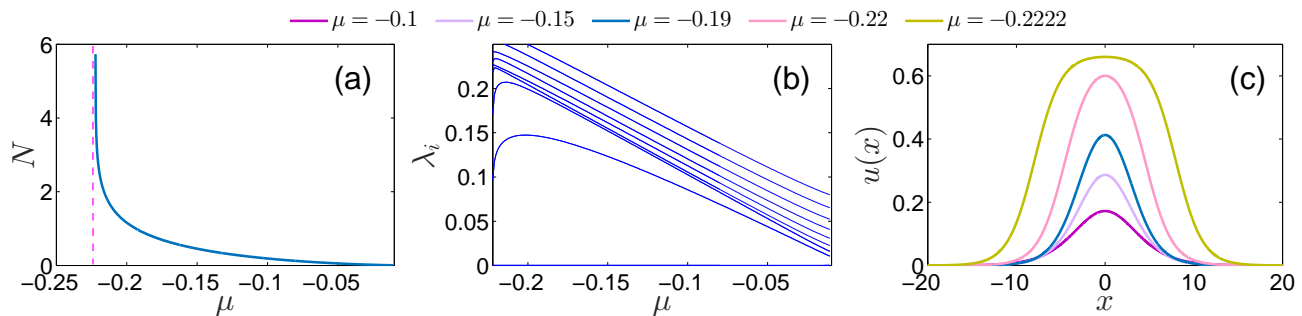


FIG. 2. (a) Numerically obtained scaled atom number for the droplet solution as a function of the chemical potential. An increase of N occurs when tending to the transition point below which only bubbles exist. This behavior is in accordance to the analytical prediction of Eq. (9). (b) The imaginary part of the linearization eigenvalues, λ_i , is depicted with respect to μ . Spectral stability, whereby $\lambda_r \equiv 0$, can be inferred independently of μ lying within the bright droplet regime. (c) Bright droplet waveforms for different values of μ (see legend) deforming from a quasi-Gaussian profile as $\mu \rightarrow 0^-$ to a flat-top configuration as $\mu \rightarrow -2/9$. These shapes and overall trend are in excellent agreement, as they should, with the exact solution of Eq. (7).

transposition), and a temporal part proportional to $e^{\lambda t}$, leads to an eigenvalue problem whose solution enables the consideration of the spectral stability of the obtained solutions, as we will discuss in further detail below.

III. STABILITY ANALYSIS FOR DROPLETS

The droplet solution of Eq. (3),

$$u_{\text{droplet}}(x) = \frac{\frac{2}{3} \frac{\mu}{\mu_0}}{1 + \sqrt{1 - \frac{\mu}{\mu_0}} \cosh(\sqrt{-2\mu}(x - x_0))}, \quad (7)$$

with $\mu_0 \equiv -2/9$, exists in the interval of $\mu_0 < \mu < 0$ [14]. In the limit of $\mu = \mu_0$, the droplet turns into a kink solution, which connects the asymptotically constant values, $u = 0$ and $u = 2/3$, fixed at $x \rightarrow \pm\infty$ [14, 23]:

$$u_{\text{kink}}(x) = \frac{1}{3} \left[1 + \tanh\left(\frac{x}{3}\right) \right]. \quad (8)$$

The scaled number of atoms in the droplet, $N = \int_{-\infty}^{+\infty} u^2(x) dx$, is

$$N_{\text{droplet}} = \frac{4}{9} \sqrt{\frac{-2}{\mu_0}} \left[\ln \left(\frac{1 + \sqrt{\frac{\mu}{\mu_0}}}{\sqrt{1 - \frac{\mu}{\mu_0}}} \right) - \sqrt{\frac{\mu}{\mu_0}} \right]. \quad (9)$$

The latter is provided in Fig. 2(a) as a function of the chemical potential. Evidently, it diverges as $\mu \rightarrow \mu_0$ and decays to zero as $\mu \rightarrow 0^-$.

The BdG spectrum assuming the above-mentioned separation of variables, namely $f = e^{\lambda t} \tilde{f}$ and $g = e^{\lambda t} \tilde{g}$ in Eqs. (6) with eigenvalues $\lambda = \lambda_r + i\lambda_i$ is presented in Fig. 2(b). Notice that all eigenvalues remain imaginary confirming the spectral stability of the bright droplet throughout its region of existence. We do not dwell on the relevant result and the bifurcation of internal modes of the bright droplet stemming from the band edge of the

continuous spectrum at $\lambda_i = \mu$ since the relevant features have been analyzed in Ref. [14]. Characteristic profiles of the bright droplet solution for varying values of μ are shown in Fig. 2(c). The bright droplet changes its shape from a Gaussian ($\mu \rightarrow 0^-$) to a flat-top ($\mu \rightarrow \mu_0^+$) configuration for decreasing μ .

IV. STATIONARY BUBBLES

We subsequently investigate bubbles appearing for $-1/4 < \mu < \mu_0 = -2/9$, see also Fig. 1(a). Utilizing the first integral formulation of the relevant quadrature problem of Eqs. (3)–(5), the relevant solution can be obtained via

$$\int \frac{du}{\sqrt{2(E - V(u))}} = \pm(x - x_0). \quad (10)$$

The bubble is represented by the homoclinic orbit attached to $u = u_+$, with mechanical energy $E = V(u_+)$ [see Eq. (4)], which can be obtained through the substitution $w = u - u_+$. A direct calculation, as expected, shows that the quantity under the radical in Eq. (10) can be rewritten in a quadratic form with respect to w ,

$$E - V(w) = \frac{w^2}{2} (A + Bw + w^2),$$

where $A \equiv 1 + 4\mu + \sqrt{1 + 4\mu} > 0$ and $B \equiv 2(1 + 3\sqrt{1 + 4\mu})/3 > 0$. The evaluation of the integral, see Ref. [46], leads to the exact analytical expression for a bubble centered at $x = x_0$

$$u_{\text{bubble}}(x) = u_+ - \frac{2A}{B + C \cosh(\sqrt{A}(x - x_0))}, \quad (11)$$

with $C \equiv \sqrt{B^2 - 4A}$. The complementary mass of the bubble,

$$N_c \equiv \int_{-\infty}^{+\infty} (u_+^2 - u^2(x)) dx, \quad (12)$$

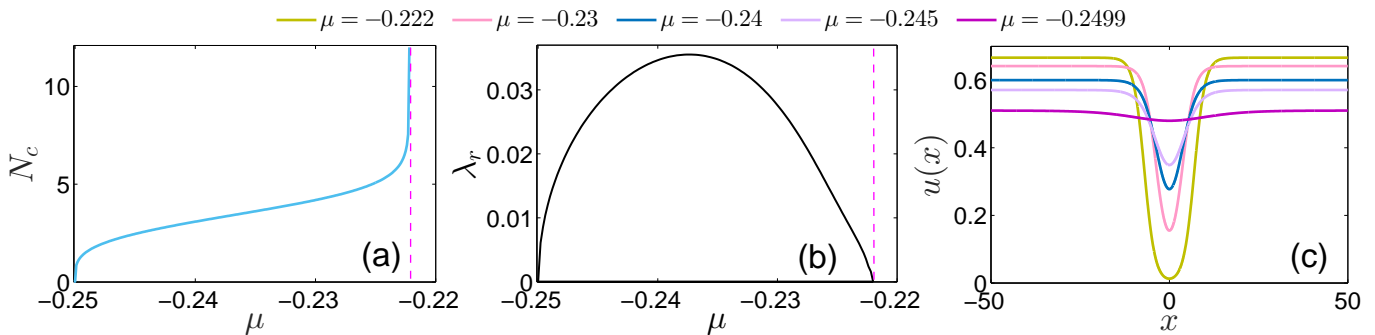


FIG. 3. (a) Complementary scaled atom number, N_c , see also Eq. (12), for a bubble stationary state in terms of μ . (b) The real part of the BdG spectrum upon chemical potential variation demonstrating the unstable nature of bubbles throughout their domain of existence. Dashed magenta lines in both (a) and (b) mark the boundary above which bubbles cease to exist. (c) The wave function of bubbles for distinct μ values (see legend). As it can be seen, for smaller $|\mu|$, the bubble's core becomes deeper, tending to be infinitely broad in the limit of $\mu \rightarrow -1/4$.

is shown as a function of μ in Fig. 3(a). As it can be seen, $N_c \rightarrow 0$ as $\mu \rightarrow -1/4$ since the relevant bubble profile becomes nearly homogeneous [see Fig. 3(c) for $\mu = -0.2499$ just before the branch disappearance] while it diverges in the limit of $\mu \rightarrow \mu_0 = -2/9$ where the bubble core is the deepest. The progressive modification of this solution towards a homogeneous (flat) one as μ increases is also presented in Fig. 3(c). The above-described trend of N_c is reminiscent of the one found for bright droplets but in terms of N [Fig. 2(a)].

The underlying stability properties of a single bubble upon chemical potential variations are depicted in Fig. 3(b). Specifically, only the real eigenvalues, λ_r , versus μ are illustrated demonstrating the spectral *instability* of this configuration throughout its interval of existence. For instance, the unstable eigenvalues for the limit bubble solutions, i.e., for $\mu = -0.2499$ and $\mu = -0.2222$ are $(\lambda_r, \lambda_i) = (0.0276, 0)$ and $(\lambda_r, \lambda_i) = (0.0043, 0)$, respectively. We remark that the time at which the instability dynamically manifests itself is inversely proportional to the magnitude of the ensuing eigenvalue. Our findings are supported by the results of Refs. [44, 45] arguing that in NLS settings bearing multi-stability, bubble-like states when they exist are always unstable.

Applying the arguments of Refs. [44, 45] to the present case, we note the following. The stationary wave function u_0 satisfies $L_1 u_0 = 0$, however $u_0 \notin L^2(\mathbb{R})$, given the asymptotics of the bubble. Accordingly, 0 is not an eigenvalue of L_1 , hence the range of L_1 is dense in $L^2(\mathbb{R})$ and we can define the inverse operator L_1^{-1} as an unbounded one with a dense domain in $L^2(\mathbb{R})$ [44, 45]. Indeed Ref. [45] proves in Lemma 3.2 that L_1 is a positive operator, i.e., $(L_1 u, u) > 0$ holds for all $u \in H^1(\mathbb{R})$. On the other hand, it is straightforward to use the Sturm-Liouville theory to prove that L_2 has a negative eigenvalue. This is because the derivative of the bubble, du_0/dx , is an odd function in $L^2(\mathbb{R})$ with a single node satisfying $L_2(du_0/dx) = 0$. Hence, the Sturm comparison theorem for this self-adjoint operator establishes the

existence of a nodeless negative eigenfunction. The combination of the two statements leads to Theorem 3.1 in Ref. [45], which suggests that in that case the eigenvalue problem represented by Eqs. (6) can be written as

$$\begin{aligned} \lambda^2 L_1^{-1} f &= -L_2 f \\ \Rightarrow \lambda^2 &= - \inf_{u \in H^1(\mathbb{R}) \cap D(L_1^{-1})} \frac{\langle L_2 f, f \rangle}{\langle L_1^{-1} f, f \rangle}. \end{aligned} \quad (13)$$

Furthermore, one can establish an upper bound of the relevant eigenvalue as $-\lambda^2 < \beta^2/4$, where $\beta = \sup[-2u_0^2(x)F'(u_0^2(x))]$ [45]. The corresponding existence of an eigenvector such that the fraction in Eq. (13) is negative confirms the existence of an associated eigenvalue pair with $\lambda^2 > 0$ which, in turn, renders the bubble generically unstable. It is interesting to contra-distinct the present case with the solitary waves vanishing at $x \rightarrow \pm\infty$, in which case 0 is an eigenvalue of L_1 [47]. This point explains the difference between the instability of the bubbles and the stability of the droplets. An interpretation of such instability provided, e.g., in the work of Ref. [44] has to do with the metastability of the relevant configuration, in comparison with the global minimum of the energy, involving the homogeneous state with vanishing amplitude. This is reflected also in the unstable dynamics of the state to which we will return in the next section. However, the difference between that and the stable dark soliton configuration lies in the effective topological protection of the latter (due to its phase jump) that precludes its destabilization, contrary to what we will see below for the bubbles.

V. DYNAMICS AND INTERACTIONS OF DROPLETS

A. Droplet collisions and Manton's method

Next, we explore the dynamics of multiple droplets with phase differences $\Delta\theta$ ranging from $\Delta\theta = 0$ (in-

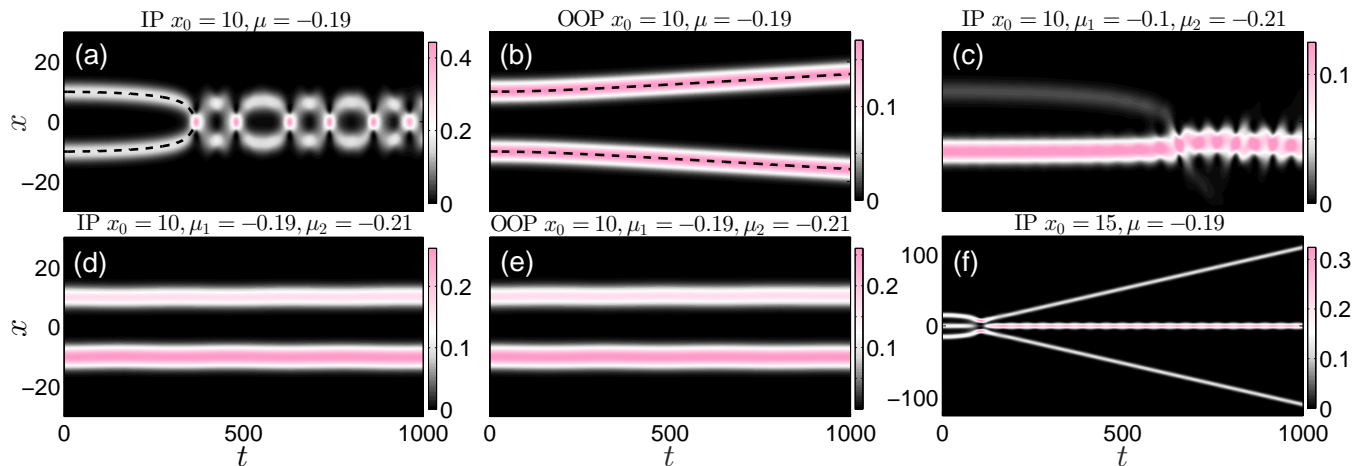


FIG. 4. (a)–(e) Spatiotemporal evolution of the density of two bright droplets, initially at rest, placed symmetrically with respect to $x = 0$ at $x = \pm x_0$, with different relative phases ($\Delta\theta = 0$ or π), and chemical potentials μ_1, μ_2 (see legends). It is evident that (a) in-phase (IP) bright droplets bearing the same μ feature attraction, whilst (b) out-of-phase (OOP) ones repel. In contrast, particle-imbalanced droplets either being (d) IP or (e) OOP remain nearly intact for small chemical potential differences. (c) Highly imbalanced IP droplets experience enhanced particle transfer. Dashed black lines indicate the prediction of the respective Manton’s method which is in excellent agreement with the simulations of Eq. (2). (f) Density dynamics of three identical IP bright droplets leading to a central, heavier and excited droplet and two lighter counter-propagating ones.

phase) to $\Delta\theta = \pi$ (out-of-phase) in analogy with what has been experimentally probed for bright solitons [48]. To examine the interactions between identical in- and out-of-phase droplets, we develop the Manton’s method [31] following the analysis reported in Ref. [30] for the NLS model. This method deploys the conservation laws for the scaled atom number, N , as well as the linear momentum,

$$P = \frac{i}{2} \int_{-\infty}^{+\infty} (uu_x^* - u^*u_x) dx. \quad (14)$$

The basic idea is that, given the conservation laws associated with N and P , the calculation of their rates of change will result in contributions stemming purely from the surface terms produced by the corresponding fluxes within the respective conservation laws. Therefore, evaluating dP/dt in a spatial domain between points a and b , and using the equation of motion, leads to

$$\frac{dP}{dt} = \frac{1}{4} \left[uu_{xx}^* + u^*u_{xx} - 2|u_x|^2 \right]_a^b. \quad (15)$$

On the other hand, dP/dt amounts to a force. Then, if one assumes the presence of two droplets centered at $x_0 = 0$ and $x_0 = s$ and considering $a < 0 < b \ll s$, with sufficiently large $|a|$ and b , the expression in Eq. (15) mostly garners a contribution from the right boundary, since the left one, at $x = a$, is exponentially weaker. As such, the only “force” at $x = b$ stems from the interaction of the droplet at $x_0 = 0$ with that at $x_0 = s$. Utilizing the asymptotic form of the two droplets, namely $u_1 = \eta e^{-\sqrt{-2\mu}x}$ and $u_2 = \eta e^{i\Delta\theta} e^{\sqrt{-2\mu}(x-s)}$, for the region near $x = b$, and using the ansatz $u = u_1 + u_2$

[where $\Delta\theta$ is the phase shift between the two droplets and $\eta \equiv \mu/(3\mu_0\sqrt{1 - \mu/\mu_0})$], one arrives at the effective force

$$\frac{dP}{dt} = -4\mu\eta^2 \cos(\Delta\theta) e^{-\sqrt{-2\mu}s}. \quad (16)$$

Subsequently, following the arguments of Ref. [30], it is possible to derive the following evolution equation for the relative position between the droplets:

$$\frac{d^2s}{dt^2} = -\frac{2}{N} \frac{dP}{dt}. \quad (17)$$

Here, the separation, s , between the two droplets has been taken into account, as well as the fact that the mass of each droplet is given by Eq. (9), while the force takes the form of Eq. (16). Notice that the relative phase appears to play a similar role as in the case of regular bright solitary waves [30, 48], *viz.*, in-phase interaction leads to attraction, while an out-of-phase one leads to repulsion. A similar approximation for the interaction between 2D and 3D solitons was elaborated in Ref. [49].

Commenting more generally on the applicability of the method, we note the following. In principle, Manton’s method can be applied when the model possesses an invariance with respect to translation that leads to the existence of a momentum conservation law. In addition, the model needs to possess solitary waves that feature an exponential tail and effective particle dynamics, as is the case with numerous one-dimensional models that bear solitons or solitary waves or even (exponentially decaying in space) breather solutions. At the moment, we are not familiar with applications of the (standard Manton) method in models that are not translationally invariant

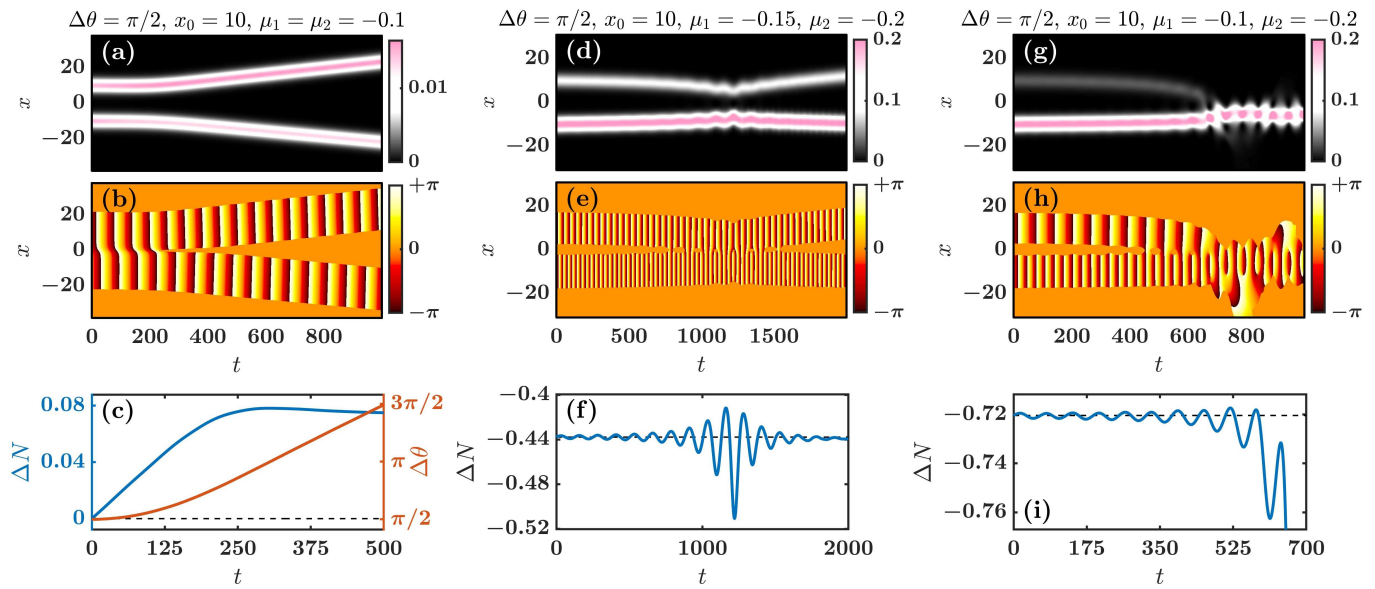


FIG. 5. Temporal evolution of two interacting droplets possessing a phase difference $\Delta\theta = \pi/2$ and initial separation $\Delta x_0 \equiv 2x_0 = 20$. Panels (a) and (b) depict, respectively, the spatio-temporal evolution of the density, $|\psi(x,t)|^2$, and phase of two identical droplets with $\mu_1 = \mu_2 = -0.1$ while panel (c) presents the corresponding time-evolution of the mass imbalance $\Delta N(t)$ [see Eq. (18)] and the relative phase, $\Delta\theta(t)$, between the two droplets. (d)–(f) The same as (a)–(c) but for the case where the initially seeded droplets have different chemical potentials, i.e. $\mu_1 = -0.15$ and $\mu_2 = -0.2$. (g)–(i) Similar to (d)–(f) but for larger chemical potential differences, namely $\mu_1 = -0.1$ and $\mu_2 = -0.2$. In all cases, transfer of mass among the droplets takes place.

or ones in which the waves feature power law tails. For the latter, recently, a far more elaborate method was introduced for capturing their interactions in Ref. [50], yet to the best of our knowledge, this has not been systematized including in higher dimensional settings as of yet. The latter clearly constitutes an interesting direction for further explorations.

The dynamical prediction of Eq. (17) has been tested for the case of in-phase (IP) bright droplet attraction [Fig. 4(a)], as well as in that of out-of-phase (OOP) droplet repulsion [Fig. 4(b)]. Here, droplets are originally ($t = 0$) placed at a relative distance $\Delta x_0 = 20$. The overall phenomenology is essentially the same for different Δx_0 . It is evident that the time-evolved density, $|\psi(x,t)|^2$, as captured by the amended GPE model of Eq. (2) is in excellent agreement with the analytical estimate of the particle picture as concerns the droplet motion. This analytical estimate is obtained upon integrating Eq. (17) and is directly compared with the attractive and the repulsive case, see dashed black lines in Fig. 4(a) and (b) respectively. It is also relevant to point out that in the case where the droplets attract, Eq. (17) is utilized up to the point where the droplets lose their individual character by approaching each other at distances comparable to their individual widths. In that regime, our assumption put forth for the Manton method (in terms of $a \ll 0 \ll b \ll s$) is no longer valid and we cannot aspire to describe the relevant dynamics accurately. Nevertheless, it is observed that in-phase droplets upon collision attempt to separate, yet cannot escape each other's at-

traction and collide anew for sufficiently long times, a pattern that recurs throughout the evolution. On the other hand, the repulsion of OOP droplets leads them to indefinite separation.

To gain an overview of the droplet's dynamical response and interactions, situations where the two bright droplets pertain to unequal chemical potentials, i.e., $\mu_1 \neq \mu_2$ are also explored. This scenario is shown in Figs. 4(c), (d), and (e). Focusing on relatively small chemical potential differences depicted in Figs. 4(d) and (e), e.g., $\mu_1 = -0.19$ and $\mu_2 = -0.21$, it is found that irrespectively of the relative phase ($\Delta\theta = 0, \pi$) a quasi-stationary state occurs persisting for all evolution times ($t \sim 5 \times 10^3$). For instance, it can be seen that even for in-phase interactions with the two droplets initialized at the same distance as before, the relevant force is *much* weaker, not allowing to infer its definitive nature. Further increase of the chemical potential imbalance which is effectively related to the number-of-atoms, i.e., mass imbalance between the droplets, results in a drastically altered dynamics, see Fig. 4(c). Particularly, the in-phase droplet collision entails a significant transfer of mass from the lighter to the heavier one. Transfer of mass has been also reported in droplet collisions with finite relative velocity [37]. Moreover, it turns out from the amended GPE predictions that imbalanced droplets experience weaker attraction than balanced ones as it can be inferred from the later occurrence of the relevant collision event, compare Figs. 4(a) and (c). This inelastic process leads to the merger of the colliding objects into

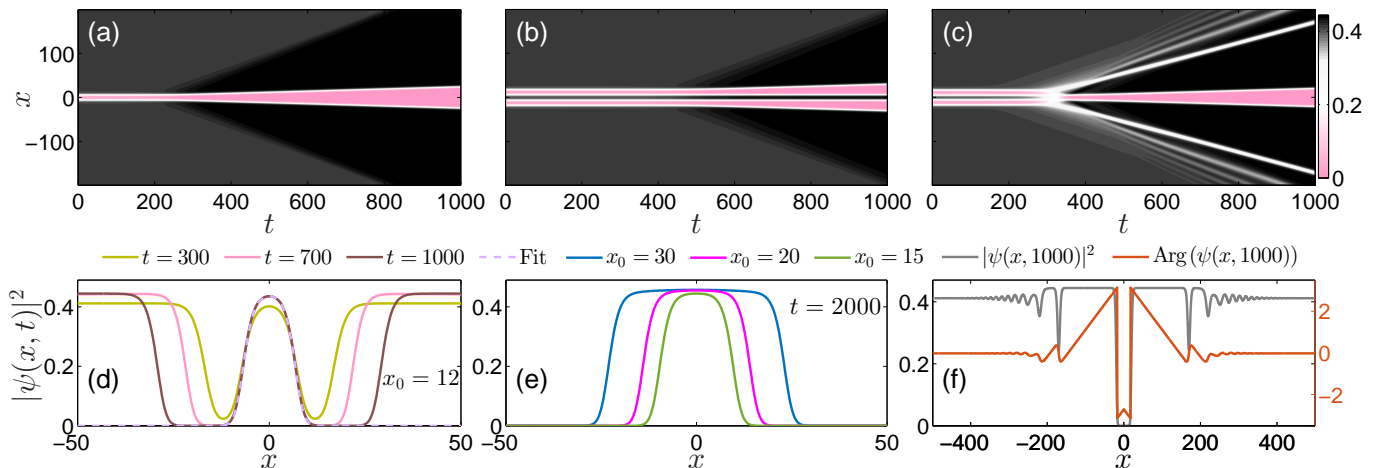


FIG. 6. (a) Density evolution of a single bubble for $\mu = -0.23$. The unstable dynamics of the bubble manifests through the expansion of its core. Dynamics of the density of two in-phase bubbles placed at a relative distance (b) $\Delta x_0 = 24$ and (c) $\Delta x_0 = 22$ exposing the crucial role of Δx_0 . Namely, for relatively small Δx_0 the bubbles attract before destabilizing generating a heavier central bubble while emitting counter-propagating shock waves leaving behind gray solitons, see in panel (f) the corresponding profile and phase at $t = 1000$. Slightly larger distances lead to non-interacting bubbles whose cores expand in the course of the evolution trapping in between a droplet as illustrated in panel (d) at distinct time-instants for $\Delta x_0 = 24$ and in (e) at a specific time-instant and varying initial separation (see legends). Dashed line in panel (d) refers to a fit of the numerically obtained waveform to the analytical droplet solution given by Eq. (7).

a single droplet in an excited state. Recall that droplet mergers can also be observed in a different context during the process of the so-called modulation instability mechanism [20, 21].

As a next step, we investigate situations with a larger number of droplets. A scenario of this sort is illustrated in Fig. 4(f), consisting of a three droplet pair-wise in-phase initialization. It is found that the collision of the three identical (particle balanced) droplets appears to occur significantly faster compared to the two droplet case [Fig. 4(a)] even though they are initially placed at larger distances. This is natural to expect on the basis of the enhanced attraction arising in the present case. Partial transfer of mass from the side droplets to the central one takes place producing two lighter and thus faster counter-propagating ones and a heavier central droplet in an excited state, which then exhibits breathing evolution. These findings motivate further studies and possible future work on the collisional dynamics of multi-droplet lattices, as such scenarios have been experimentally implemented in the realm, e.g., of dark solitons in the work of Ref. [51].

To further understand the role that the phase difference plays on droplet interactions, we additionally explored the dynamics for different values of the phase shift between the two droplets [see Fig. 5]. Phase differences between 0 and $\pi/2$ manifest an initial attraction as predicted by the effective force of Eq. (16) within the particle picture. Interestingly, it is observed that the droplets experience a slow mass exchange during their interaction. Note that the mass transfer among initially identical droplets implies symmetry breaking between them.

An explanation for this effect in soliton-soliton collisions, which can also be conceptually considered relevant to the present setting, was proposed in Ref. [52]. This involves the mismatch in the profiles' density centers and the mismatch in their phase centers, leading, in turn, to the dynamical manifestation of a symmetry-breaking. In our setting, this mass exchange is responsible for the modification of the chemical potential of the individual droplets. Specifically, the droplet with the largest $|\mu|$ will advance its phase faster than the other one, see for instance Figs. 5(e) and (h). As a result, in the course of the evolution, $\Delta\theta(t)$ becomes larger than $\pi/2$ and eventually reaches $\Delta\theta = \pi$. Therefore, the droplets will experience repulsion. A characteristic example where two droplets with an initial phase difference $\Delta\theta = \pi/2$, corresponding to a zero mutual force according to the particle picture, start exchanging mass and, around $t \approx 250$, their phase difference gets closer to $\Delta\theta = \pi$ which leads to the droplets repelling each other is showcased in Fig. 5(b), (c). The inter-droplet mass exchange is quantified by defining the mass imbalance parameter $-1 \leq \Delta N \leq 1$ as follows:

$$N_+(t) = \int_0^{+\infty} |\psi|^2 dx, \quad N_-(t) = \int_{-\infty}^0 |\psi|^2 dx,$$

$$\Delta N(t) = \frac{N_+(t) - N_-(t)}{N_+(t) + N_-(t)}. \quad (18)$$

Here, $\Delta N(t) = 0$ corresponds to a mass-balanced scenario and $\Delta N(t) > 0$ ($\Delta N(t) < 0$) to the right (left) droplet being more massive. Exploring other cases with $0 < \Delta\theta < \pi/2$ (not shown for brevity), an initial attraction was indeed observed for droplets initialized with the

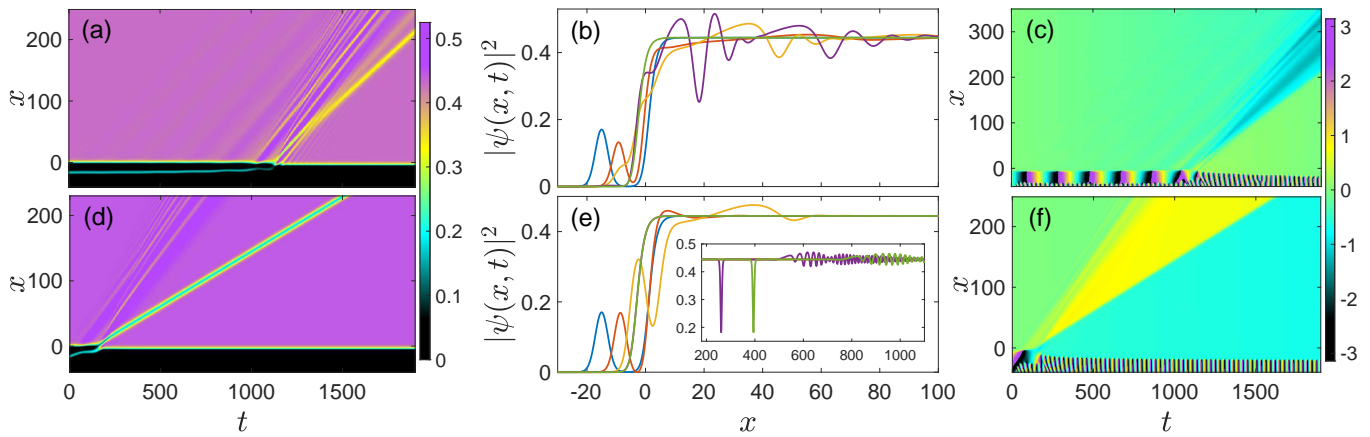


FIG. 7. (a) Density evolution for the interaction of a kink placed at $x = 0$ with a bright droplet placed at $x_0 = 15$ while having (a) zero and (d) finite velocity $v = 0.1$. (b) [(e)] Corresponding instantaneous profiles of (a) [(d)] at $t = 0$ (blue line), $t = 1023$ (orange line), $t = 1128$ (yellow line), $t = 1176$ (purple line) and $t = 1800$ (green line) [$t = 0$ (blue line), $t = 68$ (orange line), $t = 165$ (yellow line), $t = 1200$ (purple line), and $t = 1800$ (green line)]. (c) [(f)] Dynamics of the wave function's phase, $\text{Arg}(\psi)$, for case (a) [(d)]. The collision leads to the “absorption” of the droplet by the kink accompanied by the excitation of the latter and the spontaneous emission of dispersive shock waves [see also the inset in panel (e)] leaving behind a robustly propagating gray soliton [captured by the characteristic phase jump in panel (f)].

same chemical potentials in accordance with the particle picture. However, the mass imbalance generally led to an eventual repulsion of the droplets. This phenomenology is absent for $0 < \Delta\theta \ll 1$ where attraction is prevalent inducing droplet collisions similarly to the recurrent collisional events observed for IP ($\Delta\theta = 0$) identical (mass balanced) droplets presented in Fig. 4(a). Additionally, for $\pi/2 < \Delta\theta < \pi$ repulsion dominates the dynamics (not shown here).

Paradigmatic droplet interactions where the droplets are initialized bearing different masses (i.e., distinct chemical potentials) are illustrated in Fig. 5(d)–(f) for $\mu_1 = -0.15, \mu_2 = -0.2$ and Fig. 5(g)–(i) with $\mu_1 = -0.1, \mu_2 = -0.2$. In both cases oscillation of the mass imbalance [Fig. 5(f), (i)] is accompanied by a weak attraction between the droplets [Fig. 5(d), (g)] until their collision where both processes are enhanced. Particularly, for increasing chemical potential imbalances a definitive collision point can be inferred leading to a perfect mass transfer and the generation of a merger, i.e. a heavier and excited single droplet as shown in Fig. 5(g). However, in the case of smaller initial chemical potential imbalance, the droplets do not experience a clear collision point (i.e. they reach a minimum distance) before separating, see Fig. 5(d). According to the above discussion the interaction dynamics between droplets with $0 < \Delta\theta < \pi/2$, intrinsically involves mass exchange and strongly depends on the initial separation, relative phases, and chemical potentials. It is important to mention that the particle picture that was presented above is valid under the assumption of equal chemical potentials between the two droplets. Therefore, if one is to cast a particle picture for non-mass-balanced droplets a different approach is necessary and, indeed, worth developing. Efforts to better understand more general droplet interactions, together

with their corresponding particle picture, fall outside of the scope of the present work and will be reported elsewhere.

B. Dynamics of bubbles and their interactions

Having established the instability of the bubbles in their entire existence interval [see Fig. 3(b)], we proceed to explore their instability-driven dynamics. To this end, we monitor the evolution of these configurations in the framework of the amended GPE of Eq. (2), as presented in Fig. 6(a) for the single bubble and Figs. 6(b) and (c) for two bubbles. Note that, when addressing configurations including two or more bubbles, the necessity to match the backgrounds makes it possible to consider solely bubbles with equal chemical potentials, so that they asymptote to the same background value, u_+ [see Eq. (11)]. In this case, a natural ansatz is $\psi(x, t = 0) = u_0(x - x_0) \times u_0(x + x_0)/u_+$ where $x_0 = \Delta x_0/2$ is half the separation between the bubbles and $u_0(x)$ is given by the single-bubble analytical solution as described by Eq. (11).

The dynamics depicted in Fig. 6(a) suggest that, in line with the analysis of the general bubble dynamics provided in Refs. [44, 45], the inherent instability experienced by a single bubble causes it to modify its width, eventually leading it to a continuous expansion. Naturally, to maintain the total-mass conservation, the evolution leads to a slight increase of the height of the background supporting the bubble. It is interesting to note that this dynamical response is inherently related to the used Neumann or periodic boundary conditions, while it is naturally expected to be modified in the presence of

hard-wall boundaries due to the fixed background.

On the other hand, in the case of two bubbles it is observed that the ensuing interaction depends crucially on their relative distance. Placing the bubbles sufficiently far apart, their individual instability arises before they have the opportunity to interact with each other [Fig. 6(b)]. The individual core expansion persists for evolution times $t \sim 10^4$. However, it is not a symmetric expansion with respect to the center of each bubble's core. Rather, the outer part of each bubble extends as before, while in the region in between the two bubbles, a density hump is developed and trapped. We were able, upon fitting, to identify the latter as a bright droplet, see in particular Fig. 6(d). The chemical potential of the fitted droplet is $\mu = -0.2222$. Thus, the background density self-adjusts to the value corresponding to the droplet. The same dynamical bright droplet formation occurs upon further increase of the initial bubble separation as depicted in Fig. 6(e). To shed further light on the bubble interactions we then bring them in sufficient proximity that enables their interaction to commence early enough so that they merge, prior to the manifestation of their individual instability; see [Fig. 6(c)]. Evidently, an apparent attraction occurs between the two bubbles leading to a corresponding central merger and counter-propagating dispersive shock wave (DSW) structures with a downstream emission of a gray soliton train, see Fig. 6(f) [53]. This central bubble is in turn subjected to the previously discussed instability. It is also worthwhile to point out that the aforementioned emitted entities have nearly constant speed, as manifested by their nearly constant slope in the space-time contour plots of Fig. 6. This behavior can be inferred from their trajectories [see white regions in Fig. 6(c)].

C. Droplet-kink interactions

Next, we address hybrid interactions between droplets and the kink, i.e., the exact stable state given by Eq. (7) with that of Eq. (8). The droplet is initially placed at distance x_0 from the central point ($x = 0$) of the kink. Figure 7 displays examples of the ensuing interaction. In particular, the top row of panels corresponds to an initial separation $x_0 = 15$ and zero initial velocity of the droplet. The latter initially features attraction that leads to its eventual collision and “absorption”¹ by the kink occurring around $t \sim 1100$; see the details below. Figure 7(b) offers a visualization of such collision and subsequent events imprinted in the instantaneous density profiles. The collision entails intrinsic excitation of the kink. In particular, we observe spontaneous emission of a dispersive shock wave traveling through the kink background

¹ Partial reflection of the bright droplet that is of the order of 1% occurs.

and leaving behind a slower gray soliton that remains intact, despite its interaction with the former DSW while propagating. A characteristic signature of the gray soliton is produced by the evolution of the phase, $\text{Arg}(\psi)$, displayed in Fig. 7(c) which features a clear and constant phase jump. The faint ripples in $\text{Arg}(\psi)$, taking place ahead of the gray soliton signature are shock-wave imprints. In general, the droplet gets “absorbed” by the kink, subsequently leading to the emission of the above structures (DSW and gray soliton) independently of the droplet's chemical potential (quantifying its mass) and original position x_0 . Naturally, the phenomenology happens faster for heavier droplets and smaller distances (results not shown here).

This phenomenology can be generalized for droplets with initial velocity v_0 . In this case, the collision is, as expected, accelerated, as seen from the comparison of Figs. 7(a) and (d), as well as of the corresponding snapshots in Figs. 7(b) and (e). This conclusion is also supported by monitoring the phase of the wave function, in the course of the evolution, where signatures of both the shock wave (ripples) and the gray soliton (phase jump being a fraction of π) can be distinguished. In this case, the emission of the dispersive shock wave and the nucleation of the gray soliton become more conspicuous, see the inset of Fig. 7(e) where both entities are clearly captured. A more detailed study of collisions of traveling droplets with kinks or other effective scattering potentials is a relevant direction for studies beyond the scope of the present work. In this context, it will be relevant to consider related transmission and reflection phenomena as it was recently done in Ref. [39] for a droplet colliding with a square well.

D. The kink-antikink interaction

In addition to the kink waveform of Eq. (8), Eq. (3) gives rise to the antikink solution, $u_{\text{antikink}}(x) = (1/3)[1 - \tanh(x/3)]$. As such, for reasons of completeness we also examine kink-antikink interactions. The overlap in the kink-antikink pair exponentially decays with the separation between them, therefore the interaction is appreciable only for a relatively small separation (i.e., of a few times the width of the individual kink). Actually, this condition is favorable to a potential experimental realization, as a relatively small spatial domain and short timescales are required. An example, when the kink and antikink are brought in close proximity, with initial separation $\Delta x_0 = 10$, is presented in Fig. 8(a). Apparently, the kink-antikink interaction is repulsive, in line with a similar result known for the cubic-quintic NLS model [54]; we note here in passing the similarly repulsive interaction of the (kink-like) dark solitons of the standard NLS model. Specifically, repulsion [Fig. 8(b)] is accompanied by the spontaneous emission of two counter-propagating dispersive shock waves as can be identified by inspecting the density snapshots shown in Fig. 8(c).

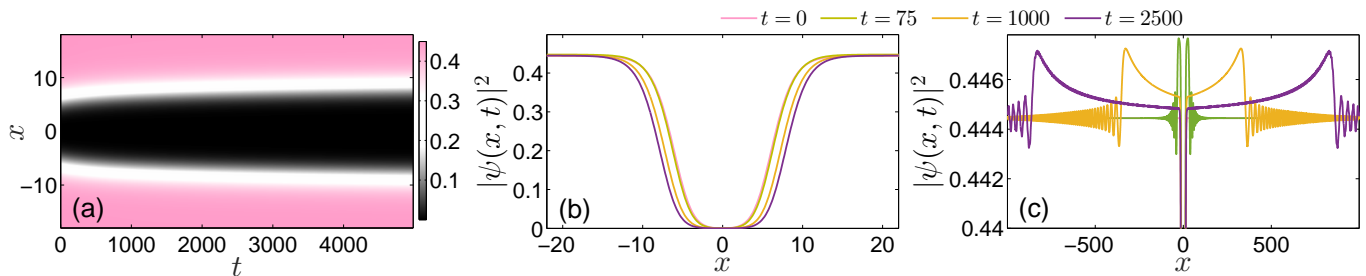


FIG. 8. (a) Spatiotemporal evolution of the density, $|\psi(x, t)|^2$, in the course of the apparently repulsive kink-antikink interaction with initial separation $\Delta x_0 = 10$. (b) Snapshots of (a) at different time-instants (see legend). (c) Magnification of (b) for visualizing the counter-propagating shock-wave emission.

We note that the repulsive nature of the interaction persists for moving kink and antikink, each one initiated by $u(x) = u_{\text{(anti)kink}}(x) + \epsilon du_{\text{(anti)kink}}(x)/dx$, with boost parameter ϵ (not shown here). Note that, in contrast to the genuinely repulsive OOP droplet-droplet interaction [Fig. 4(b)], here we deal with heteroclinic waveforms and thus the definition of the associated mass is an intriguing problem in its own right; for a recent discussion of the simpler, standard GPE problem and its dark soliton heteroclinic solutions, see, e.g., Ref. [55] and, in particular, Appendix C therein. Nevertheless, we still observe a repulsive interaction in Fig. 8(a), and the accompanying dispersive shock-wave emission leads the kinks into a slowdown that eventually halts them in line with the expectation that no traveling such solutions exist in the model under consideration.

VI. CONCLUSIONS & PERSPECTIVES

We have studied the static properties of droplets and bubbles within the one-dimensional amended GPE model relevant to the inclusion of the LHY term in homonuclear, mass-balanced, bosonic mixtures. In this context, we systematically explored the interactions among different types of nonlinear excitations. Particularly, our investigation involved multiple droplets and bubbles, but also droplet-kink and kink-antikink ones. The stability of droplets and bubbles upon chemical potential variations has been explored, expanding upon related earlier work. The parametric regions of existence of each solution were identified with droplets transitioning from Gaussian to flat-top ones for decreasing chemical potential while bubbles becoming wider and deeper. Moreover, the stability of the droplets and instability of bubbles has been demonstrated by extracting the corresponding Bogoliubov-de-Gennes excitation spectrum. The destabilization of bubbles manifests through expansion of their core in the course of the evolution.

Turning to the dynamics, interactions between droplets were found, similarly to bright solitons, to depend on their relative phase and chemical potential difference. Importantly, the particle picture for droplets is constructed revealing their in-phase attraction and out-

of-phase repulsion. This outcome is subsequently tested by monitoring the interactions of these entities through the amended GPE model. Additionally, we showcase that for intermediate phase differences droplets initially experience attraction followed by repulsion. The interaction between droplets with different chemical potentials leads to mass exchange between them and the formation of heavier droplets in an excited state.

On the other hand, bubble interactions, given the bubbles' individual, unstable nature are highly susceptible to different outcomes depending on their initial separation. Particularly, if placed in close proximity, they merge into a single bubble due to their mutual attraction followed by the emission of counter-propagating shock waves and the subsequent formation of gray soliton trains. However, for slightly increased separation they show individual core expansion trapping in between them a droplet. Examining interactions among kinks and droplets reveals the transformation of the latter by the former accompanied by the spontaneous generation of a dispersive shock wave leaving behind a gray soliton. These dynamical features are enhanced for traveling or lighter droplets. We have also explored kink-antikink interactions which generically result in mutual repulsion and emission of weak counter-propagating shock waves.

Our findings suggest pathways for further work. A direct extension is to consider a quasi-1D geometry, aiming to reveal the role of transversal excitations in colliding droplets and bubbles. This is an effort that it appears to us would be particularly useful towards connecting with experimental settings (including in the presence of external confinement). Also, a detailed analysis of the emitted shock-wave structures following the droplet-kink collision is an issue of substantial interest. The generalization of the “two-body” particle-like dynamical picture developed herein for droplets and bubbles to 1D *chains* of such structures is a promising prospect, producing potentially effective dynamical lattice equations similar to the ones for dark and bright NLS solitons described in Ref. [56]. Other relevant directions are to further quantify the analytical characterization of inter-soliton interactions (of different type), as well as to study interactions and collisions between solitons and/or vortical droplets in the 2D setting combining the mean-field and LHY terms, and,

on the other hand, in full quantum states (beyond the limits of the LHY description) [57–59].

ACKNOWLEDGEMENTS

S.I.M. acknowledges support from the NSF through a grant for ITAMP at Harvard University. This ma-

terial is based upon work supported by the U.S. National Science Foundation under awards PHY-2110038 (R.C.G.) and PHY-2110030 and DMS-2204702 (P.G.K.). The work of B.A.M. was supported, in part, by the Israel Science Foundation through grant No. 1695/22.

-
- [1] D. S. Petrov, *Phys. Rev. Lett.* **115**, 155302 (2015).
- [2] A. Khan and A. Debnath, *Frontiers in Physics* , 534 (2022).
- [3] M. Schmitt, M. Wenzel, F. Böttcher, I. Ferrier-Barbut, and T. Pfau, *Nature* **539**, 259 (2016).
- [4] L. Chomaz, I. Ferrier-Barbut, F. Ferlaino, B. Laburthe-Tolra, B. L. Lev, and T. Pfau, *Rep. Progr. Phys.* (2022).
- [5] C. R. Cabrera, L. Tanzi, J. Sanz, B. Naylor, P. Thomas, P. Cheiney, and L. Tarruell, *Science* **359**, 301 (2018).
- [6] P. Cheiney, C. R. Cabrera, J. Sanz, B. Naylor, L. Tanzi, and L. Tarruell, *Phys. Rev. Lett.* **120**, 135301 (2018).
- [7] C. D’Errico, A. Burchianti, M. Prevedelli, L. Salasnich, F. Ancilotto, M. Modugno, F. Minardi, and C. Fort, *Phys. Rev. Research* **1**, 033155 (2019).
- [8] G. Semeghini, G. Ferioli, L. Masi, C. Mazzinghi, L. Wolswijk, F. Minardi, M. Modugno, G. Modugno, M. Inguscio, and M. Fattori, *Phys. Rev. Lett.* **120**, 235301 (2018).
- [9] T. D. Lee, K. Huang, and C. N. Yang, *Phys. Rev.* **106**, 1135 (1957).
- [10] D. S. Petrov and G. E. Astrakharchik, *Phys. Rev. Lett.* **117**, 100401 (2016).
- [11] G. Ferioli, G. Semeghini, S. Terradas-Briansó, L. Masi, M. Fattori, and M. Modugno, *Phys. Rev. Research* **2**, 013269 (2020).
- [12] C. Fort and M. Modugno, *Applied Sciences* **11** (2021), 10.3390/app11020866.
- [13] S. I. Mistakidis, A. G. Volosniev, R. E. Barfknecht, T. Fogarty, T. Busch, A. Foerster, P. Schmelcher, and N. T. Zinner, arXiv preprint arXiv:2202.11071 (2022).
- [14] M. Tylutki, G. E. Astrakharchik, B. A. Malomed, and D. S. Petrov, *Phys. Rev. A* **101**, 051601(R) (2020).
- [15] I. A. Englezos, S. I. Mistakidis, and P. Schmelcher, *Phys. Rev. A* **107**, 023320 (2023).
- [16] P. Stürmer, M. N. Tengstrand, R. Sachdeva, and S. M. Reimann, *Phys. Rev. A* **103**, 053302 (2021).
- [17] A. Cappellaro, T. Macrì, and L. Salasnich, *Phys. Rev. A* **97**, 053623 (2018).
- [18] G. De Rosi, G. E. Astrakharchik, and P. Massignan, *Phys. Rev. A* **103**, 043316 (2021).
- [19] J. Wang, H. Hu, and X.-J. Liu, *New J. Phys.* **22**, 103044 (2020).
- [20] T. Mithun, A. Maluckov, K. Kasamatsu, B. A. Malomed, and A. Khare, *Symmetry* **12**, 174 (2020).
- [21] T. Mithun, S. I. Mistakidis, P. Schmelcher, and P. G. Kevrekidis, *Phys. Rev. A* **104**, 033316 (2021).
- [22] S. R. Otajonov, E. N. Tsoy, and F. K. Abdullaev, *Phys. Rev. A* **106**, 033309 (2022).
- [23] G. C. Katsimiga, S. I. Mistakidis, G. N. Koutsokostas, D. J. Frantzeskakis, R. Carretero-González, and P. G. Kevrekidis, *Phys. Rev. A* **107**, 063308 (2023).
- [24] S. Saqlain, T. Mithun, R. Carretero-González, and P. G. Kevrekidis, *Phys. Rev. A* **107**, 033310 (2023).
- [25] S. Gangwar, R. Ravisankar, P. Muruganandam, and P. K. Mishra, *Phys. Rev. A* **106**, 063315 (2022).
- [26] Y. V. Kartashov, V. M. Lashkin, M. Modugno, and L. Torner, *New J. Phys.* **24**, 073012 (2022).
- [27] M. N. Tengstrand, P. Stürmer, E. Karabulut, and S. M. Reimann, *Phys. Rev. Lett.* **123**, 160405 (2019).
- [28] M. Barranco, R. Guardiola, S. Hernández, R. Mayol, J. Navarro, and M. Pi, *J. Low Temp. Phys.* **142**, 1 (2006).
- [29] J. P. Toennies and A. F. Vilesov, *Angewandte Chemie International Edition* **43**, 2622 (2004).
- [30] P. G. Kevrekidis, A. Khare, and A. Saxena, *Phys. Rev. E* **70**, 057603 (2004).
- [31] N. S. Manton, *Nuclear Physics B* **150**, 397 (1979).
- [32] W. Zhao and E. Bourkoff, *Opt. Lett.* **14**, 1371 (1989).
- [33] G. C. Katsimiga, G. M. Koutentakis, S. I. Mistakidis, P. G. Kevrekidis, and P. Schmelcher, *New J. Phys.* **19**, 073004 (2017).
- [34] G. Ferioli, G. Semeghini, L. Masi, G. Giusti, G. Modugno, M. Inguscio, A. Gallemí, A. Recati, and M. Fattori, *Phys. Rev. Lett.* **122**, 090401 (2019).
- [35] V. Cikojević, L. V. Markić, M. Pi, M. Barranco, F. Ancilotto, and J. Boronat, *Phys. Rev. Research* **3**, 043139 (2021).
- [36] Y. Hu, Y. Fei, X.-L. Chen, and Y. Zhang, *Frontiers of Physics* **17**, 61505 (2022).
- [37] G. E. Astrakharchik and B. A. Malomed, *Phys. Rev. A* **98**, 013631 (2018).
- [38] S. Gangwar, R. Ravisankar, P. Muruganandam, and P. K. Mishra, arXiv preprint arXiv:2303.01216 (2023).
- [39] A. Debnath, A. Khan, and B. Malomed, arXiv preprint arXiv:2302.13367 (2023).
- [40] M. Edmonds, “Dark quantum droplets in beyond-mean-field Bose-Einstein condensate mixtures,” (2022).
- [41] C. Chin, R. Grimm, P. Julienne, and E. Tiesinga, *Rev. Mod. Phys.* **82**, 1225 (2010).
- [42] M. Olshanii, *Phys. Rev. Lett.* **81**, 938 (1998).
- [43] G. C. Katsimiga, S. I. Mistakidis, T. M. Bersano, M. K. H. Ome, S. M. Mossman, K. Mukherjee, P. Schmelcher, P. Engels, and P. G. Kevrekidis, *Phys. Rev. A* **102**, 023301 (2020).
- [44] I. Barashenkov, A. Gocheva, V. Makhankov, and I. Puzynin, *Physica D: Nonlinear Phenomena* **34**, 240 (1989).
- [45] A. de Bouard, *SIAM Journal on Mathematical Analysis* **26**, 566 (1995), <https://doi.org/10.1137/S0036141092237029>.
- [46] I. S. Gradshteyn and I. M. Ryzhik, *Table of Integrals, Series, and Products*, 4th ed. (Academic Press, New York, 1980).

- [47] T. Kapitula and K. Promislow, *Spectral and Dynamical Stability of Nonlinear Waves* (Springer New York, 2013).
- [48] J. H. V. Nguyen, P. Dyke, D. Luo, B. A. Malomed, and R. G. Hulet, *Nature Physics* **10**, 918 (2014).
- [49] B. Malomed, *Phys. Rev. E* **58**, 7928 (1998).
- [50] N. S. Manton, *Journal of Physics A: Mathematical and Theoretical* **52**, 065401 (2019).
- [51] G. Theocharis, A. Weller, J. P. Ronzheimer, C. Gross, M. K. Oberthaler, P. G. Kevrekidis, and D. J. Frantzeskakis, *Phys. Rev. A* **81**, 063604 (2010).
- [52] L. Khaykovich and B. Malomed, *Phys. Rev. A* **74**, 023607 (2006).
- [53] G. El and M. Hofer, *Physica D: Nonlinear Phenomena* **333**, 11 (2016), dispersive Hydrodynamics.
- [54] G. Filatrella, B. A. Malomed, and M. Salerno, *Phys. Rev. A* **90**, 043629 (2014).
- [55] G. I. Martone, A. Recati, and N. Pavloff, *Phys. Rev. Res.* **3**, 013143 (2021).
- [56] M. Ma, R. Navarro, and R. Carretero-González, *Phys. Rev. E* **93**, 022202 (2016).
- [57] L. Parisi, G. E. Astrakharchik, and S. Giorgini, *Phys. Rev. Lett.* **122**, 105302 (2019).
- [58] S. I. Mistakidis, T. Mithun, P. G. Kevrekidis, H. R. Sadeghpour, and P. Schmelcher, *Phys. Rev. Research* **3**, 043128 (2021).
- [59] M. Ota and G. Astrakharchik, *Sci. Phys.* **9**, 020 (2020).